LATVIAN JOURNAL OF PHYSICS AND TECHNICAL SCIENCES
2017, N 4

DOI: 10.1515/lpts-2017-0027

APPLIED PHYSICS

INFLUENCE OF THE PREPARATION METHOD ON PLANAR PEROVSKITE $CH_3NH_3PBI_{3-X}CL_X$ SOLAR CELL PERFORMANCE AND HYSTERESIS

A. Ivanova[1,2], A. Tokmakov[3], K. Lebedeva[1],
M. Roze[2], I. Kaulachs[1]
[1]Institute of Physical Energetics
11 Krivu Str., Riga, LV-1006, LATVIA
email: kaulacs@edi.lv
[2]Riga Technical University
14/24 Paula Valdena Str., Riga, LV-1048, LATVIA
[3]LU Institute of Solid State Physics
8 Kengaraga Str., Riga LV-1063, LATVIA

Organometal halide perovskites are promising materials for low-cost, high-efficiency solar cells. The method of perovskite layer deposition and the interfacial layers play an important role in determining the efficiency of perovskite solar cells (PSCs). In the paper, we demonstrate inverted planar perovskite solar cells where perovskite layers are deposited by two-step modified interdiffusion and one-step methods. We also demonstrate how PSC parameters change by doping of charge transport layers (CTL). We used dimethylsupoxide (DMSO) as dopant for the hole transport layer (PEDOT:PSS) but for the electron transport layer [6,6]-phenyl C_{61} butyric acid methyl ester (PCBM)) we used N,N-dimethyl-N-octadecyl(3-aminopropyl)trimethoxysilyl chloride (DMOAP).

The highest main PSC parameters (*PCE, EQE,* V_{OC}) were obtained for cells prepared by the one-step method with fast crystallization and doped CTLs but higher fill factor (*FF*) and shunt resistance (R_{sh}) values were obtained for cells prepared by the two-step method with undoped CTLs.

Keywords: *inverted structure, mixed halide cells, perovskite solar cells, planar heterojunction*

1. INTRODUCTION

Solar energy continues to be a potential source of clean, abundant and sustainable energy. The photovoltaic process is considered an ideal energy process – photovoltaics convert solar energy directly to electrical energy. In recent years, great atten-

tion has been paid to organic-inorganic hybrid halide perovskite solar cells (ABX_3, $A=CH_3NH_3$, B=Pb, Sn, X=I, Cl, Br) [1]–[7]. Miyasaka and colleagues in 2009 incorporated perovskite semiconductor in solar cell and represented solar cell with power conversion efficiency (PCE) 3.8 % [8]. Then perovskite solar cell (PSC) efficiency increased rapidly to 22.1 % [9]. Apart from their high efficiency, perovskites have many other advantages, including low cost, light weight, mechanical flexibility, semi-transparency. Perovskites emerged as highly attractive sunlight convertors for their high charge carrier mobility, high absorption coefficient and long electron- and hole-diffusion lengths [6], [10]–[12].

Performance of PSCs is closely related to the morphology and chemical composition of the perovskite absorbers [13]. The most widely studied perovskites are methylammonium triiodide lead perovskite ($CH_3NH_3PbI_3$) [2]-[4] and its mixed analogue methylammonium chloride-iodide lead perovskite ($CH_3NH_3PbI_{3-x}Cl_x$) [13], [14]. The Cl^- in precursor solution can enhance crystallinity of the resulting perovskite films. The improved carrier transport has also been observed in $MAPbI_{3-x}Cl_x$ films with carrier diffusion length exceeding 1 μm, which is one order of magnitude larger than that of $MAPbI_3$ [15]. In addition, it has been mentioned for the first time by Snaith et al. that introducing trace quantity of chlorine can dramatically improve electrical properties of perovskite materials [16]. It should also be noted that in mixed halide perovskites the carrier lifetime can be prolonged substantially to ~1 microsecond [17].

There can be two types of perovskite solar cells – mesoporous cells [11], [18]–[20], where perovskites are grown on a mesoporous oxide layer, and planar cells [4], [21], [22]. However, mesoporous devices need high temperature sintering that increases the processing time and cost of solar cell. Planar devices through a simple, scalable and low-temperature technique can make perovskite solar cells commercially viable.

The planar devices can be divided into regular (n-i-p) and inverted (p-i-n) structures depending on the selective contact used on the bottom. The general solvents used for PSC*s*, such as N,N-dimethylformamide (DMF) and dimethylsulfoxide (DMSO), have very good solubility and can wash off the most of the underlayer of perovskites. Therefore, many conventional hole transporting materials (HTL) are difficult to apply in the p-i-n type PSCs. The most used HTL in inverted type cells is poly(3,4-ethylenedioxythiophene) polysterene sulphonate (PEDOT:PSS) [23], [24]. Many inorganic oxides are also widely used, such as NiO [25], NiO_x [26], VO_x [27], CuO_x [28]. Different fullerene derivatives, such as [6,6]-phenyl C_{61} butyric acid methyl ester (PCBM), are widely used as electron transporting material in inverted perovskite solar cells [1], [23], [29]. PCBM is the commonly used ETL material due to its solution processibility, appropriate energy levels for efficient exciton dissociation, and good electron transport and hole blocking properties [30].

In the present paper, we demonstrate inverted planar heterojunction perovskite solar cells where perovskite layers are formed by the two-step modified interdiffusion and one-step methods. We also investigate how PSC parameters change by doping ETL or both ETL and HTL.

2. EXPERIMENTAL PART

Devices were fabricated with the following structures:

- ITO/PEDOT:PSS/$CH_3NH_3PbI_{3-x}Cl_x$/PCBM/C_{60}/Ag (sample N1 and N2),
- ITO/PEDOT:PSS/$CH_3NH_3PbI_{3-x}Cl_x$/PCBM:DMOAP/Ag (sample N3)
- ITO/PEDOT:PSS:DMSO/$CH_3NH_3PbI_{3-x}Cl_x$/PCBM:DMOAP/Ag (sample N4).

Device structural illustration and energy diagram of the used layers are demonstrated in Fig. 1.

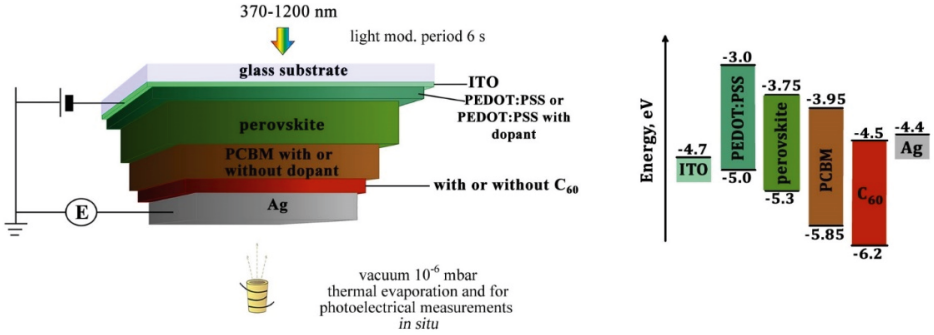

Fig. 1. Structural illustration of the studied cells and the energy level diagram of layers.

The ITO-coated glass substrates (PGO) (15 ohm/sq) were cleaned in chloroform (*Sigma Aldrich*), acetone (*Sigma Aldrich*), deionized water and isopropanol (*Sigma Aldrich*) in ultrasonic bath for 15 min in sequence and exposed to ultraviolet ozone (UVO) irradiation for 20 min. PEDOT:PSS (*Clevios Baytron AI 4083)* water solution with or without DMSO (*Sigma Aldrich*) was spin coated on ITO at a rate 5000 rpm for 60 sec at 60 °C and annealed at 145 °C for 30 min.

Then $CH_3NH_3PbI_{3-x}Cl_x$ layer was deposited by using the two methods – the two-step modified interdiffusion [31] (sample N1) and one-step [32] (samples N2, N3, N4) methods.

- Two-step modified interdiffusion method: the mixture of PbI_2 (TCI) and $PbCl_2$ (*Sigma Aldrich*) (with molar ratio 3.4) dissolved in DMF (*Sigma Aldrich*) and DMSO solvent mixture with molar ratio 3 was spin coated at a rate 6500 rpm at 65 °C for 75 s using 65 °C hot solution and was dried for 10 minutes at room temperature and for 10 minutes at 70 °C with the aim to remove remaining solvents. Methyl ammonium iodide (MAI) CH_3NH_3I (*TCI*) solution in 2-propanol (40 mg/mL) was spin coated at a rate 6000 rpm at 65 °C on top of PbI_2/$PbCl_2$ layer. The obtained bilayer system was annealed in the closed system at 100 °C for 1 h and additionally for 1 h in argon atmosphere to finish the formation of $CH_3NH_3PbI_{3-x}Cl_x$ perovskite film.
- One-step method: perovskite precursors solution in DMF was spin coated on PEDOT:PSS at a rate 6500 rpm for 60 sec at 40 °C. After a few seconds

when the spin coating process of perovskite solution was started, 200 μL anhydrous chlorobenzene (*Sigma Aldrich*) was dropped onto the centre of the substrate to induce fast crystallization [32]. The obtained film was annealed at 80 °C for 30 min and then at 100 °C for 60 min to complete the formation of $CH_3NH_3PbI_{3-x}Cl_x$ perovskite layer. After cooling down to room temperature (RT), the sample was moved into methylamine (MA) 33 wt% solution in ethanol vapours for some seconds (*Acros Organics*) to obtain smoother surface [33].

After the perovskite layer was deposited, PCBM (*Solenne*) solution in chloroform (20 mg/mL) with or without 2.5 mol% N,N-dimethyl-N-octadecyl(3-aminopropyl)trimethoxysilyl chloride (DMOAP) (*Sigma Aldrich*) was spin coated at a rate 2000 rpm for 60 sec at 40 °C and annealed at 80 °C for 30 min and then at 100 °C for 60 min. After cooling down to RT, the sample was transferred into the high vacuum chamber where C_{60} fullerene and Ag (*Kurt J. Lesker company*) electrode layers were thermally evaporated. Double fullerene layer (samples N1 and N2) was used with the aim to passivate the trap states [34]. Active cell area was 7 mm^2.

All photoelectric measurements were made in the same homemade vacuum cryostat system where C_{60} and electrode layers were thermally evaporated without breaking the vacuum and moving the cell. During the evaporation process the thickness of C_{60} and Ag electrode was controlled by a calibrated 10 MHz quartz oscillator and frequency meter. The spectral dependencies of short circuit photocurrent external quantum efficiency (EQE) were investigated in the spectral range 370–900 nm, using a synhro-detection technique and PC controlled data storage equipment [35], [36]. The samples were illuminated by chopper-modulated monochromatic light. The selected light modulation period was chosen as 6 s long and the light intensity was controlled by a calibrated Si photodiode. A constant photon flux on the sample during the measurement was achieved by a computer controlled movement of the Thorlabs linear variable optical density metallic ND filter with the correction on the Si photodiode spectral sensitivity. The dark current was checked permanently as a residual current during the end of the dark half-period of light modulation for evolution series and shunt resistances of our cells.

3. RESULTS AND DISCUSSION

Spectral dependencies of the external quantum efficiency (EQE) and optical density of photoactive layer are shown in Fig. 2. Spectral dependencies are measured at 10^{15} phot/(cm^2·s) light intensity.

EQE values grow by ~ 30 % if the preparation method of perovskite layers is changed from the two-step modified interdiffusion method to the one-step method (compare samples N1 and N2). *EQE* values grow by ~ 10 % if the electron transporting layer (ETL) PCBM is doped by DMOAP with concentration of 2.5 mol% [37]. The hydrolyzable alkoxysilane groups on DMOAP enable moisture cross-linking through the formation of stable siloxane bonds. This doped PCBM interfacial layer provides multipositive effects for the use in PSCs, including excellent film coverage on the perovskite layer, good robustness against the undersirable reaction between

the mobile iodide ions and Ag electrode, reasonable electrical conductivity, fine-tunability of WF of Ag electrode [37]. The highest *EQE* values (which exceed 90 %) can be achieved by doping both the hole transporting layer (HTL) PEDOT:PSS and ETL. DMSO as additive promotes pinhole-free perovskite layer formation. DMSO acts as a solvent of the MAPbI precursors and mediates the nucleation and crystallization at the PEDOT:PSS surface [38].

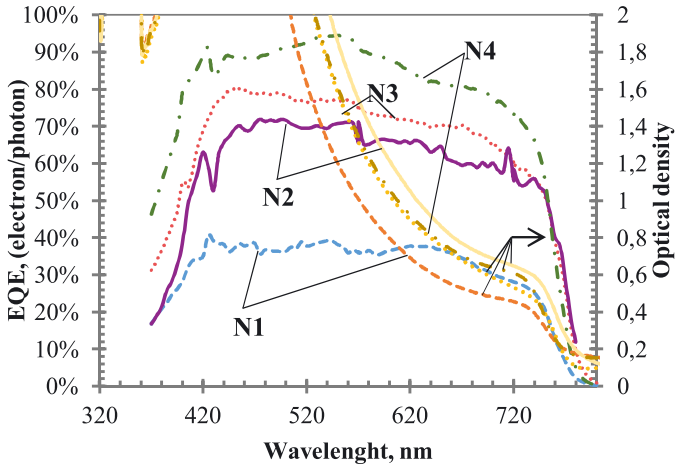

Fig 2. Spectral dependencies of the short circuit photocurrent *EQE* and optical densities of photoactive layer
(sample N1: ITO/PEDOT:PSS/perovskite (2 step method)/PCBM/C_{60}/Ag
sample N2: ITO/PEDOT:PSS/perovskite (1 step method)/PCBM/C_{60}/Ag
sample N3: ITO/PEDOT:PSS/perovskite (1 step method)/PCBM:DMOAP/Ag
sample N4: ITO/PEDOT:PSS:DMSO/perovskite (1 step method)/PCBM:DMOAP/Ag).

As it is shown in Fig. 2, samples with perovskite layers prepared by the one-step method (samples N2, N3 and N4) demonstrate higher *EQE* values than the sample with the perovskite layer prepared by the two-step modified interdiffusion method (sample N1).

The increase in *EQE* values is accompanied by the decrease in *FF* as it is shown in Fig. 3 and Table 1. Fill factor (FF) values do not exceed 0.4 for samples (N2, N3 and N4), where the perovskite layer is made by the one-step method, but for sample N1 (the perovskite layer is made by the two-step modified interdiffusion method) FF values exceed 0.58. The lowest *FF* values are observed for sample N2 (~0.3). FF values increase slightly by doping ETL (sample N3) or both *ETL* and HTL (sample N4). However, in sample N4 we observe large hysteresis, in samples N1, N2 and N3 hysteresis practically is insignificant (Fig. 3). R_{shunt} values are about an order smaller for sample N4 than in sample N2 and N3 and about two orders than in sample N1.

The highest open circuit voltage (V_{OC}) values are observed for samples where the perovskite layer is made by the one-step method (for sample N4, where both EHL and HTL are doped), V_{OC} value is 1.1 V. But for sample N1 V_{OC} value is only 0.86 V.

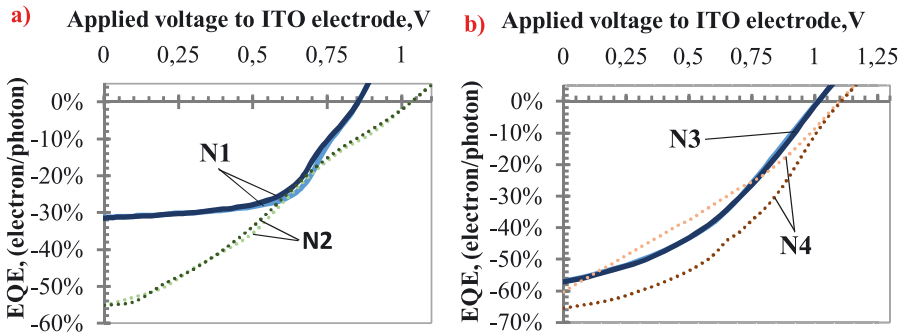

Fig. 3. Photocurrent *EQE* dependencies on the applied external voltage at 720 nm and light intensity 10^{15} phot/(cm^2·s) for:

a) samples N1 and N2;

b) samples N3 and N4.

(Lighter curves are measured at increasing voltage, darker – at decreasing voltage, "-" sign at *EQE* values denotes photocurrent direction indicating that electrons are going to upper Ag electrode.)

Table 1

Characteristics of Measured Samples at 720 nm and at Light Intensity 10^{15} phot/(cm^2·s) Obtained at Increasing Voltage (→) and Decreasing Voltage (←)

	EQE		*Voc, V*		*FF*		*PCE*	
	→	←	→	←	→	←	→	←
N1	0.279	0.282	0.856	0.859	0.583	0.534	8.10 %	7.52 %
N2	0.552	0.551	1.034	1.034	0.312	0.296	10.35 %	9.80 %
N3	0.568	0.572	1.012	1.014	0.396	0.391	13.23 %	13.16 %
N4	0.604	0.655	1.097	1.105	0.295	0.402	11.36 %	16.89 %

Table 2

Shunt and Series Resistances Measured from Residual Dark Current during Light Modulation at 720 nm and at Light Intensity 10^{15} phot/(cm^2·s) Obtained at Increasing Voltage (→) and Decreasing Voltage (←)

	R_{shunt}, Ω		R_{series}, Ω	
	→	←	→	←
N1	2.50E+07	2.38E+07	4.80E+02	4.81E+02
N2	3.46E+06	3.40E+05	5.32E+03	5.15E+03
N3	2.94E+06	3.45E+06	1.10E+03	1.11E+03
N4	3.10E+05	5.20E+05	4.34E+02	4.52E+02

The power conversion efficiency (*PCE*) is calculated according to formula 1 [35].

$$PCE = \frac{V_{OC} \cdot FF \cdot EQE}{E_{phot}}, \quad (1)$$

where V_{OC} – open circuit voltage, V;
FF – fill factor;
EQE – external quantum efficiency for short circuit photocurrent;
E_{phot} – energy of photon, eV.

PCE spectral dependencies are shown in Fig. 4. The higher *PCE* values are observed by using the one-step method for preparing the perovskite layer and they exceed 10 % even for undoped *CTLs* (Fig. 4a). When the ETL is doped, *PCE* increases to 12–14 %. If both HTL and ETL are doped, *PCE* increases up to 16–17 % (Fig. 4b), but in this case we observe very strong hysteresis (sample N4 in Fig. 4b), possibly by trap states which are formed in the layers when *ETL* and HTL are doped.

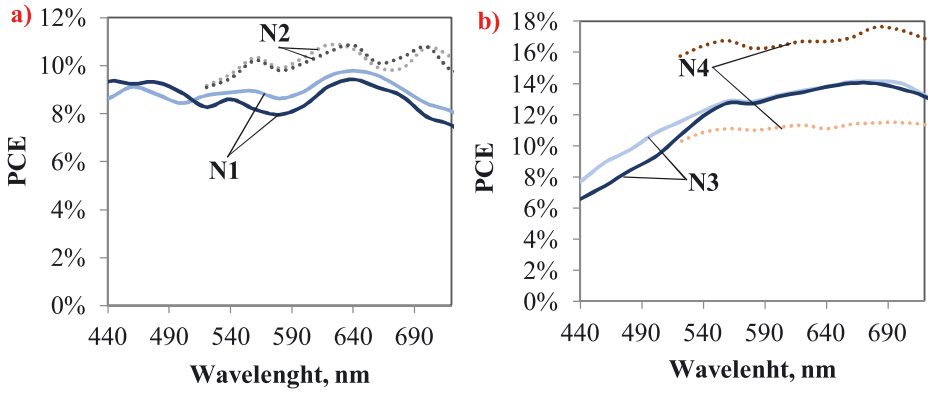

Fig. 4. Spectral dependencies of power conversion efficiency (*PCE*) at light intensity 10^{15} phot/(cm^2·s) for:
a) samples N1 and N2;
b) samples N3 and N4.
(Lighter curves are measured at increasing voltage, darker – at decreasing voltage.)

4. CONCLUSIONS

We have reported on four planar heterojunction systems, where perovskite layers are formed by using the two-step modified interdiffusion and one-step methods and where ETL or both ETL and HTL are doped. We have found that

- higher *EQE*, V_{OC} and *PCE* values are observed, when the perovskite layer is formed by using the one-step method employing fast crystallization;
- higher *FF* and R_{sh} values are observed, when the perovskite layer is formed by using the two-step modified interdiffusion method without doping *CTLs*;
- when both ETL and HTL are doped, strong hysteresis is observed in current-voltage and *PCE* spectral dependencies possibly by too high carrier trap concentration.

ACKNOWLEDGEMENTS

The present research has been supported by the State Research Programme "LATENERGI" and National Research Programme "Multifunctional Materials and Composites, Photonics and Nanotechnology (IMIS2)".

REFERENCES

1. Bretschneider, S. A., Weickert, J., Dorman, J. A., & Schmidt-Mende, L. (2014). Research update: physical and electrical characteristics of lead halide perovskites for solar cell applications. *APL Mater.*, 2(5), 40701. DOI: 10.1063/1.4871795.
2. Burschka, J., Pellet, N., Moon, S.-J., Humphry-Baker, R., Gao, P., Nazeeruddin, M. K., & Grätzel, M. (2013). Sequential deposition as a route to high-performance perovskite-sensitized solar cells. *Nature*, 499(7458), 316–320. DOI: 10.1038/nature12340.
3. Heo, J. H., Im, S. H., Noh, J. H., Mandal, T. N., Lim, C.-S., Chang, J. A., Lee, Y. H., Kim, H., Sarkar, A., Nazeeruddin, M. K., Gratzel, M., & Il Seok, S. (2013). Efficient inorganic-organic hybrid heterojunction solar cells containing perovskite compound and polymeric hole conductors. *Nat. Photonics*, 7(6), 486–491. DOI: 10.1038/nphoton.2013.80 efficient.
4. Liu, D., & Kelly, T. L. (2013). Perovskite solar cells with a planar heterojunction structure prepared using room-temperature solution processing techniques. *Nat. Photonics*, 8(2), 133–138. DOI: 10.1038/nphoton.2013.342.
5. Lotsch, B. V. (2014). New light on an old story: perovskites go solar. *Angew. Chemie - Int. Ed.*, 53(3), 635–637. DOI: 10.1002/anie.201309368.
6. Niu, G., Guo, X., & Wang, L. (2015). Review of recent progress in chemical stability of perovskite solar cells. *J. Mater. Chem. A*, 3(17), 8970–8980. DOI: 10.1039/c4ta04994b.
7. Ibn-Mohammed, T., Koh, S.C.L., Reaney, I.M, Acquaye, A., Schileo, G., Mustapha, K.B., &Greenough, R. (2017). Perovskite solar cells: an integrated hybrid lifecycle assessment and review in comparison with other photovoltaic technologies. *Renew. Sus. Energy Rev.*, 80, 1321-1344. DOI: 10.1016/j.rser.2017.05.095
8. Kojima, A., Teshima, K., Shirai, Y., & Miyasaka, T. (2009). Organometal halide perovskites as visible-light sensitizers for photovoltaic cells. *J. Am. Chem. Soc.*, 131(17), 6050–6051. DOI: 10.1021/ja809598r.
9. NREL, "Efficiency Chart," *Nrel*. p. 1, 2017.
10. Mehmood, U., Al-Ahmed, A., Afzaal, M., Al-Sulaiman, F. A., & Daud, M. (2017). Recent progress and remaining challenges in organometallic halides based perovskite solar cells. *Renew. Sustain. Energy Rev.*, 78, 1–14. DOI: 10.1016/j.rser.2017.04.105.
11. Mei, A., Li, X., Liu, L., Ku, Z., Liu, T., Rong, Y., Xu, M., Hu, M., Chen, J., Yang, Y., Grätzel, M., & Han, H. (2014). A hole-conductor–free, fully printable mesoscopic perovskite solar cell with high stability. *Science*, 345(6194), 295–298. DOI: 10.1126/science.1254763.
12. Yang, W. S., Noh, J. H., Jeon, N. J., Kim, Y. C., Ryu, S., Seo, J., & Il Seok, S. (2015). High-performance photovoltaic perovskite layers fabricated through intramolecular exchange. *Science*, 348(6240), 1234–1237. DOI: 10.1126/science.aaa9272.
13. Eperon, G. E., Burlakov, V. M., Docampo, P., Goriely, A., & Snaith, H. J. (2014). Morphological control for high performance, solution-processed planar heterojunction perovskite solar cells. *Adv. Funct. Mater.*, 24(1), 151–157. DOI: 10.1002/adfm.201302090.

14. Heo, J. H., & Im, S. H. (2016). Highly reproducible, efficient hysteresis-less $CH_3NH_3PbI_{3-x}Cl_x$ planar hybrid solar cells without requiring heat-treatment. *Nanoscale*, 8(2554–2560). DOI: 10.1039/c5nr08458j.
15. Qing, J., Chandran, H. T., Cheng, Y., Liu, K., Li, H.-W., Tsang, S. W., Lo, M.-F., & Lee, C.-S. (2015). Chlorine incorporation for enhanced performance of planar perovskite solar cell based on lead acetate precursor. *ACS Appl. Mater. Interfaces*, 7(41), 23110–23116. DOI: 10.1021/acsami.5b06819.
16. 16. Quilettes, D. W., Vorpahl, S. M., Stranks, S. D., Nagaoka, H., Eperon, G. E., Ziffer, M. E., Snaith, H. J., & Ginger, D. S. (2015). Impact of microstructure on local carrier lifetime in perovskite solar cells. *Science*, 348(6235), 683–686. DOI: 10.1126/science.aaa5333
17. Fan, L., Ding, Y., Luo, J., Shi, B., Yao, X., Wei, C., Zhang, D., Wang, G., Sheng, Y., Chen, Y., Hagfeldt, A., Zhao, Y., & Zhang, X. (2017). Elucidating the role of chlorine in perovskite solar cells. *J. Mater. Chem. A*, 5, 7423–7432. DOI: 10.1039/c7ta00973a.
18. Lee, M. M., Teuscher, J., Miyasaka, T., Murakami, T. N., & Snaith, H. J. (2012). Efficient hybrid solar cells based on meso-superstructured organometal halide perovskites. *Science*, 338(6107), 643–647. DOI: 10.1126/science.1228604 [doi].
19. Zhao, Y., Nardes, A. M., & Zhu, K. (2014). Mesoporous perovskite solar cells: material composition, charge-carrier dynamics, and device characteristics. *Faraday Discuss.*, 176, 301–312. DOI: 10.1039/c4fd00128a.
20. Di Giacomo, F., Zardetto, V., Lucarelli, G., Cinà, L., Di Carlo, A., Creatore, M., & Brown, T. M. (2016). Mesoporous perovskie solar cells and the role of nanoscale compact layers for remarkable all-round high efficiency under both indoor and outdoor illummination. *Nano Energy*, 30, 460–469. DOI: 10.1016/j.nanoen.2016.10.030.
21. Liu, M., Johnston, M. B., & Snaith, H. J. (2013). Efficient planar heterojunction perovskite solar cells by vapour deposition. *Nature*, 501, 395–398. DOI: 10.1038/nature12509.
22. Tan, H., Jain, A., Voznyy, O., Lan, X., Yuan, M., Zhang, B., Zhao, Y., Fan, F., Li, P., Quan, L. N., Zhao, Y., Lu, Z., Yang, Z., Hoogland, S., & Sargent, E. H. (2017). Efficient and stable solution-processed planar perovskite solar cells via contact passivation. *Science*, 355, 722–726. DOI: 10.1126/science.aai9081
23. Seo, J., Park, S., Kim, Y. C., Jeon, N. J., Noh, J. H., Yoon, S. C., & Il Seok, S. (2014). Benefits of very thin PCBM and LiF layers for solution-processed p-i-n perovskite solar cells. *Energy Environ. Sci.*, 7(8), 2642–2646. DOI: 10.1039/c4ee01216j.
24. Docampo, P., Ball, J. M., Darwich, M., Eperon, G. E., & Snaith, H. J. (2013). Efficient organometal trihalide perovskite planar-heterojunction solar cells on flexible polymer substrates. *Nat. Commun.*, 4, 2761. DOI: 10.1038/ncomms3761.
25. Seo, S., Park, I. J., Kim, M., Lee, S., Bae, C., Jung, H. S., Park, N. G., Kim, J. Y., & Shin, H. (2016). An ultra-thin, un-doped NiO hole transporting layer of highly efficient (16.4%) organic-inorganic hybrid perovskite solar cells. *Nanoscale*, 8(22), 11403–11412. DOI: 10.1039/c6nr01601d.
26. Yin, X., Que, M., Xing, Y., & Que, W. (2015). High efficiency hysteresis-less inverted planar heterojunction perovskite solar cells with a solution-derived NiO_x hole contact layer. *J. Mater. Chem. A*, 3(48), 24495–24503. DOI: 10.1039/c5ta08193a.
27. Xiao, M., Gao, M., Huang, F., Pascoe, A. R., Qin, T., Cheng, B., Bach, U., & Spiccia, L. (2016). Efficient perovskite solar cells employing inorganic interlayers. *ChemNanoMat*, 2(3), 182–188. DOI: 10.1002/cnma.201500223.
28. Rao, H., Ye, S., Sun, W., Yan, W., Li, Y., Peng, H., Liu, Z., Bian, Z., Li, Y.,& Huang, C. (2016). A 19.0 % efficiency achieved in CuO_x-based inverted $CH_3NH_3PbI_{3-x}Cl_x$ solar

cells by an effective Cl doping method. *Nano Energy*, 27, 51–57. DOI: 10.1016/j.nanoen.2016.06.044.

29. Li, M., Shen, P., Wang, K., Guo, T., & Chen, P. (2015). Inorganic p-type contact materials for perovskite-based solar cells. *J. Mater. Chem. A.*, 3(17), 9011–9019. DOI: 10.1039/c4ta06425a.
30. Gao, P., Gratzel, M., & Nazeeruddin, M. K. (2014). Organohalide lead perovskites for photovoltaic applications. *Energy Environ. Sci.*, 7, 2448–2463. DOI: 10.1039/c4ee00942h.
31. Xiao, Z., Bi, C., Shao, Y., Dong, Q., Wang, Q., Yuan, Y., Wang, C., Gao, Y., & Huang, J. (2014). Efficient, high yield perovskite photovoltaic devices grown by interdiffusion of solution-processed precursor stacking layers. *Energy Environ. Sci.*, 7(8), 2619. DOI: 10.1039/c4ee01138d.
32. Ye, S., Rao, H., Yan, W., Li, Y., Sun, W., Peng, H., Liu, Z., Bian, Z., Li, Y., & Huang, C. (2016). A strategy to simplify the preparation process of perovskite solar cells by co-deposition of a hole-conductor and a perovskite layer. *Adv. Mater.*, 28(43), 9648–9654. DOI: 10.1002/adma.201603850.
33. Zhou, Z., Wang, Z., Zhou, Y., Pang, S., Wang, D., Xu, H., Liu, Z., Padture, N. P., & Cui, G. (2015). Methylamine-gas-induced defect-healing behavior of $CH_3NH_3PbI_3$ thin films for perovskite solar cells. *Angew. Chemie Int. Ed.*, 54(33), 9705–9709. DOI: 10.1002/anie.201504379.
34. Wang, Q., Yuan, Y., & Huang, J. (2014). Large fill-factor bilayer iodine perovskite solar cells fabricated by a low-temperature solution-process. *Energy Environ. Sci.*, 7, 359–2365. DOI: 10.1039/c4ee00233d.
35. Kaulachs, I., Muzikante, I., Gerca, L., Shlihta, G., Shipkovs, P., Grehovs, V., Kalnachs, J., Roze, M., Rozite, G., & Ivanova, A. (2013). Electrodes for GaOHPc:PCBM/P3HT:PCBM bulk heterojunction solar cell. *Chem. Phys.*, 405, 46–51. DOI: 10.1016/j.chemphys.2012.06.007.
36. Kaulachs, I., & Silinsh, E. (1994). Molecular triplet exciton generation via optical charge transfer states in a-metalfree phthalocyanine, studied by magnetic field effects. *Latv. J. Phys. Tech. Sci.*, 5, 12–22, 1994.
37. Chang, C., Huang, W., & Chang, Y. (2016). Highly-efficient and long-term stable perovsite solar cells enabled by a cross-linkable n-doped cathode interfacial layer. *Chem. Mater.*, 28, 6305–6312. DOI: 10.1021/acs.chemmater.6b02583.
38. Kaltenbrunner, M., Adam, G., Głowacki, E. D., Drack, M., Schwödiauer, R., Leonat, L., Apaydin, D. H., Groiss, H., Scharber, M. C., White, M. S., Sariciftci, N. S., & Bauer, S. (2015). Flexible high power-per-weight perovskite solar cells with chromium oxide-metal contacts for improved stability in air. *Nat. Mater.*, 14, 1032–1039. DOI: 10.1038/nmat4388.

IZGATAVOŠANAS METODES IETEKME UZ PLĀNĀRO PEROVSKĪTA $CH_3NH_3PBI_{3-X}CL_X$ SAULES ELEMENTU PARAMETRIEM UN HISTERĒZI

A. Ivanova, A. Tokmakov, K. Ļebedeva, M. Roze, I. Kaulačs

K o p s a v i l k u m s

Organometāliskie halogenīdu perovskīti ir daudzsološs materiāls lētu augsti efektīvu saules elementu izveidei. Perovskīta slāņa uznešanas metode un starpslāņu izvēle stipri ietekmē perovskīta saules elementu efektivitāti. Šajā darbā mēs demonstrējam inversās planārās perovskīta saules šūnas, kurās perovskīta slānis tiek veidots, izmantojot modificētu interdifūzijas divpakāpju vai vienpakāpes metodes. Ka arī mēs parādam, kā perovskīta saules elementu parametri mainās atkarībā no lādiņa transportslāņu dopēšanas. Caurumu transportslānim (PEDOT:PSS) kā dopantu mēs izmantojām dimetilsulfoksīdu (DMSO), bet elektronu transportslānim ([6,6]-fenil C_{61} sviestskābes metilesterim (PCBM)) N,N-dimetil-N-oktadecil(3-aminopropil)trimetoksisilil hlorīdu (DMOAP).

Augstākas *PCE*, *EQE* un V_{OC} vērtības tika sasniegtas šūnām, kurās perovskīta slānis tika veidots, izmantojot vienpakāpes metodi ar paātrināto kristalizāciju un dopētiem lādiņa transporta slāņiem, bet augstākas *FF* un R_{sh} vērtības – šūnām, kurās perovskīta slānis veidots, izmantojot divpakāpju metodi, un ar nedopētiem lādiņa transporta slāņiem.

15.07.2017.

Institute of Solid State Physics, University of Latvia as the Center of Excellence has received funding from the European Union's Horizon 2020 Framework Programme H2020-WIDESPREAD-01-2016-2017-TeamingPhase2 under grant agreement No. 739508, project CAMART²